

## Stability and etching of titanium oxynitride films in hydrogen microwave plasma

Hien Do, Tzu-Chun Yen, and Li Chang

Citation: *Journal of Vacuum Science & Technology A* **31**, 041304 (2013); doi: 10.1116/1.4811676

View online: <http://dx.doi.org/10.1116/1.4811676>

View Table of Contents: <http://scitation.aip.org/content/avs/journal/jvsta/31/4?ver=pdfcov>

Published by the AVS: Science & Technology of Materials, Interfaces, and Processing

---

### Articles you may be interested in

Differences in erosion mechanism and selectivity between Ti and TiN in fluorocarbon plasmas for dielectric etch

*J. Vac. Sci. Technol. B* **30**, 041811 (2012); 10.1116/1.4736979

Electrostatic quadrupole plasma mass spectrometer measurements during thin film depositions using simultaneous matrix assisted pulsed laser evaporation and magnetron sputtering

*J. Vac. Sci. Technol. A* **28**, 419 (2010); 10.1116/1.3372401

Tungsten metal gate etching in Cl<sub>2</sub>/O<sub>2</sub> inductively coupled high density plasmas

*J. Vac. Sci. Technol. B* **26**, 1875 (2008); 10.1116/1.3002392

Investigation of etching properties of metal nitride/high-*k* gate stacks using inductively coupled plasma

*J. Vac. Sci. Technol. A* **23**, 964 (2005); 10.1116/1.1927536

Etching characteristics of platinum in inductively coupled plasma using Cl<sub>2</sub>/CO

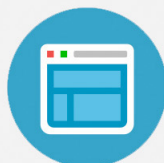
*J. Vac. Sci. Technol. B* **22**, 1662 (2004); 10.1116/1.1761310

---



## Re-register for Table of Content Alerts

Create a profile.



Sign up today!



# Stability and etching of titanium oxynitride films in hydrogen microwave plasma

Hien Do,<sup>a)</sup> Tzu-Chun Yen, and Li Chang

Department of Materials Science and Engineering, National Chiao Tung University, Hsinchu 1001, Taiwan 300

(Received 10 March 2013; accepted 5 June 2013; published 20 June 2013)

Epitaxial titanium oxynitride (TiNO) films deposited on MgO by pulsed laser deposition were treated in hydrogen microwave plasma. Scanning electron microscopy and x-ray photoelectron spectroscopy were used to examine the stability and etching of TiNO which strongly depended on hydrogen gas pressure. TiNO was very chemically stable and remained with good crystallinity under hydrogen pressure below 5300 Pa. With increase of pressure, it may lead to the formation of etch pits in inverse pyramid shape. The etch mechanism as well as the effects of gas pressure and etching time are also presented. © 2013 American Vacuum Society. [<http://dx.doi.org/10.1116/1.4811676>]

## I. INTRODUCTION

Titanium nitride (TiN) possesses many excellent mechanical and physical properties such as high melting point, hardness and chemical stability, good electrical and thermal conductivity, and high corrosion and oxidation resistance.<sup>1</sup> Therefore, TiN has been widely applied as a hard coating material for tools and a new hard mask for etching of materials with low etch rate such as magnetic films and transition metals.<sup>2,3</sup> TiN is also often used in microelectronic devices as conductive diffusion barrier between Si and interconnection metals such as Al and Cu for multilevel metallization.<sup>4–8</sup> Also, TiN can act as antireflection layer in microelectronic fabrication.<sup>9–11</sup> Therefore, TiN films may come across subsequent etching processes.

Most of TiN films have been deposited mainly by chemical vapor deposition, pulsed laser deposition (PLD), and magnetron sputtering. In such deposition processes, residual oxygen was found to strongly react with titanium due to high affinity between them, even under very high vacuum.<sup>12–14</sup> Therefore, most of the deposited films were found to be titanium oxynitride (TiNO). The incorporation of oxygen into TiN films has beneficial effects on diffusion barrier performance for Al<sup>15,16</sup> but often induces increase in the resistivity of the film. A nitrogen/hydrogen or pure nitrogen plasma treatment has been used to improve the crystallinity and electrical conductivity of polycrystalline TiNO films due to its capability to reduce oxygen and carbon concentration.<sup>14,17,18</sup> Surface cleaning of TiN/TiNO by hydrogen plasma has been applied for Al metallization in multilevel microelectronic fabrication.<sup>19</sup> Also, reactive ion etching of TiN-based films has often used gases containing hydrogen in plasma such as Cl<sub>2</sub>/CHF<sub>3</sub>, Cl<sub>2</sub>/Ar/CHF<sub>3</sub>, Cl<sub>2</sub>/N<sub>2</sub>/CHF<sub>3</sub>, Ar/CHF<sub>3</sub>, and CH<sub>4</sub>/H<sub>2</sub>.<sup>6,20</sup> However, treatment of TiNO by pure hydrogen plasma has been rarely studied. TiN and TiNO have been also applied in hydrogen environment; but there is still a lack of understanding about the effect of hydrogen on those materials. Therefore, the effects of atomic hydrogen on the surface structure and chemical composition

of TiNO should be taken into consideration because any change in structure and chemical composition can affect properties of TiNO. Furthermore, studying the etching of TiNO by pure hydrogen plasma could be helpful for the first understanding about the role of hydrogen in the patterning process using plasma containing atomic hydrogen as mentioned above.<sup>6,20</sup> Furthermore, though hydrogen plasma treatment have been applied to the revelation of dislocation etch pits in many materials,<sup>21</sup> there are no similar reports on TiNO.

Here we report the study of the effects of pure hydrogen microwave plasma on the stability and etching of TiNO films as function of gas pressure and time. The high-quality epitaxial TiNO films were used in our study due to the lack of bulk single crystals TiNO, and it can avoid the complicated etch effects from grain boundaries and orientations in polycrystalline films. It is also noticed that the use of high-quality epitaxial TiNO films in many applications can improve electrical properties and remove the problems of fast grain boundary diffusion of dopants and impurities in the polycrystalline films of columnar grains.<sup>22</sup> The etch mechanism and the changes in chemical composition and surface morphology were also investigated.

## II. EXPERIMENT

Epitaxial (001) titanium oxynitride films were grown on MgO(001) substrates by using PLD method. Before the deposition, a 5-cm MgO(001) substrate was ultrasonically cleaned in acetone, dried with nitrogen gas, and immediately loaded into the vacuum chamber with base pressure of  $133 \times 10^{-6}$  Pa. The substrate was faced a 5-cm titanium oxynitride (TiNO<sub>0.064</sub>) target at a distance of 14 cm. The target was irradiated with a KrF ( $\lambda = 248$  nm) laser beam at an angle of 45° and rotated during deposition. After the substrate was heat-treated at 700 °C for 1800 s, the deposition process was then carried out under the condition as follows: laser pulse repetition rate of 10 Hz, laser power density  $\sim 2\text{--}3 \times 10^4$  J/m<sup>2</sup>, and substrate temperature  $\sim 700$  °C. After the deposition process had been completed, the substrate was cooled down to room temperature in 5400 s in vacuum. The deposited films were then placed on a molybdenum

<sup>a)</sup>Electronic mail: dohienvl@gmail.com

TABLE I. Hydrogen plasma treatment parameters.

Sample	Pressure (Pa)	Time (s)
A	5300	5400
B	8000	1800
C	10 700	1800
D	10 700	3600
E	10 700	9000

holder and loaded into a 2.45 GHz/5 kW ASTeX-type microwave plasma chemical vapor deposition reactor.<sup>23</sup> The plasma was then generated under hydrogen gas ambient with flow rate of 300 sccm and microwave power of 1000 W. The hydrogen plasma treatment was done at gas pressure varied from 5300 to 10 700 Pa and treatment time varied from 1800 to 9000 s (details in Table I). In the reactor, the increase in pressure caused the volume of the plasma ball to shrink, which in turn increased the plasma density.<sup>24</sup> During the treatment, the substrate temperature determined by optical pyrometer increased from 900 to 1100 °C with pressure increasing from 5300 to 10 700 Pa. After the plasma was switched off, the sample was cooled down to room temperature in about 600 s. The surface morphology of the films was then examined with atomic force microscopy (AFM) (D3100, Digital Instruments Inc.). TiNO/MgO interface was observed in cross-section by using scanning electron microscopy (SEM) (JEOL JSM-6500F-SEM). Chemical compositions of the TiNO films before and after plasma treatment were determined by employing x-ray photoelectron spectroscopy (XPS) (ULVAC-PHI, PHI Quantera SXM) using a monochromatic Al K $\alpha$  radiation source. High-resolution x-ray diffractometry (Bede D1) was used to investigate the change in the crystallinity, thickness, density, and strain state of the thin films. The Bede D1 system was equipped a two-bounce Si 220 channel-cut collimator crystal, a dual channel Si 220 analyzer crystal, and CuK $\alpha_1$  radiation ( $\lambda = 0.15406$  nm).

### III. RESULTS AND DISCUSSION

The epitaxial growth of (001)TiNO on MgO was determined by x-ray diffraction (XRD) with cube-on-cube orientation of TiNO(001)//MgO(001) and TiNO[100]//MgO[100]. The film thickness was measured to be about 76 nm. The microstructure, electrical, and mechanical properties have been characterized, which are shown elsewhere.<sup>22</sup>

The surface morphology of as-grown and hydrogen plasma treated samples A, B, C, D, and E (Table I) was examined with AFM. As seen clearly in Fig. 1, the surface of the TiNO film treated for 5400 s at pressure of 5300 Pa (sample A) shows almost no etch pits, but it becomes slightly rougher with root-mean-square (rms) roughness of 0.48 nm compared with 0.32 nm for the as-grown TiNO. However, TiNO becomes etched at pressure of 8000–10 700 Pa for a treatment time of 1800 s (Fig. 2). The AFM image in the inset of Fig. 2(a) with its corresponding section analysis shows that the etched TiNO surface morphology appears with inverse pyramid etch pits which have the edges of the

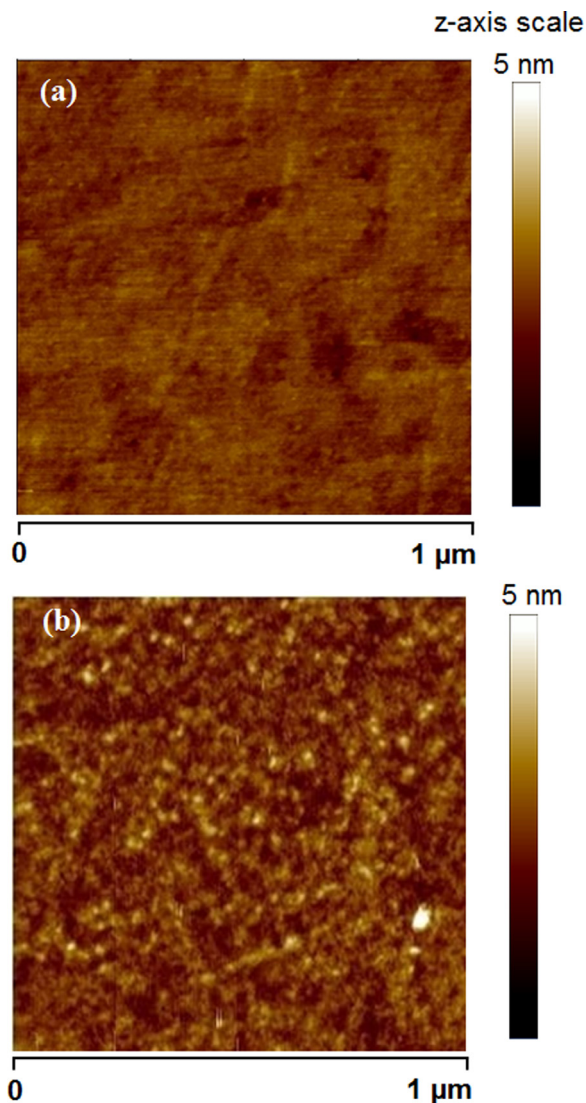


FIG. 1. (Color online) AFM images of (a) as-grown TiNO films and (b) TiNO film after hydrogen plasma treatment at pressure of 5300 Pa for 5400 s (sample A). Z-axis is for color scale.

pyramid parallel to  $\langle 100 \rangle$  direction of the epitaxial TiNO films. The etch size and etch depth are defined as shown in the drawing of the pyramid. The origin of pyramid etch pits in TiNO films can be explained as in NaCl structure. Mandelson<sup>25</sup> has demonstrated that in NaCl crystal, the etch pits of inverse pyramid are produced at intersections of dislocations with the surface. Similarly, it is possible that the inverse pyramid etch pits appearing on our TiNO films are associated with dislocation sites. Indeed, as shown later in XRD data, the dislocation density can be estimated from x-ray rocking curve broadening (full width half at maximum 230 arcsec) to be around  $10^8$  cm $^{-2}$  that is similar to the etch pit density observed on AFM images. AFM images also show that no particles left on the surface, indicating the complete removal of etch products after etching.

The distribution of etch size and etch depth for samples treated at different pressure and etching time are shown in histograms of Fig. 3. It is found that the etch size and the etch depth are increased with pressure and etching time. The

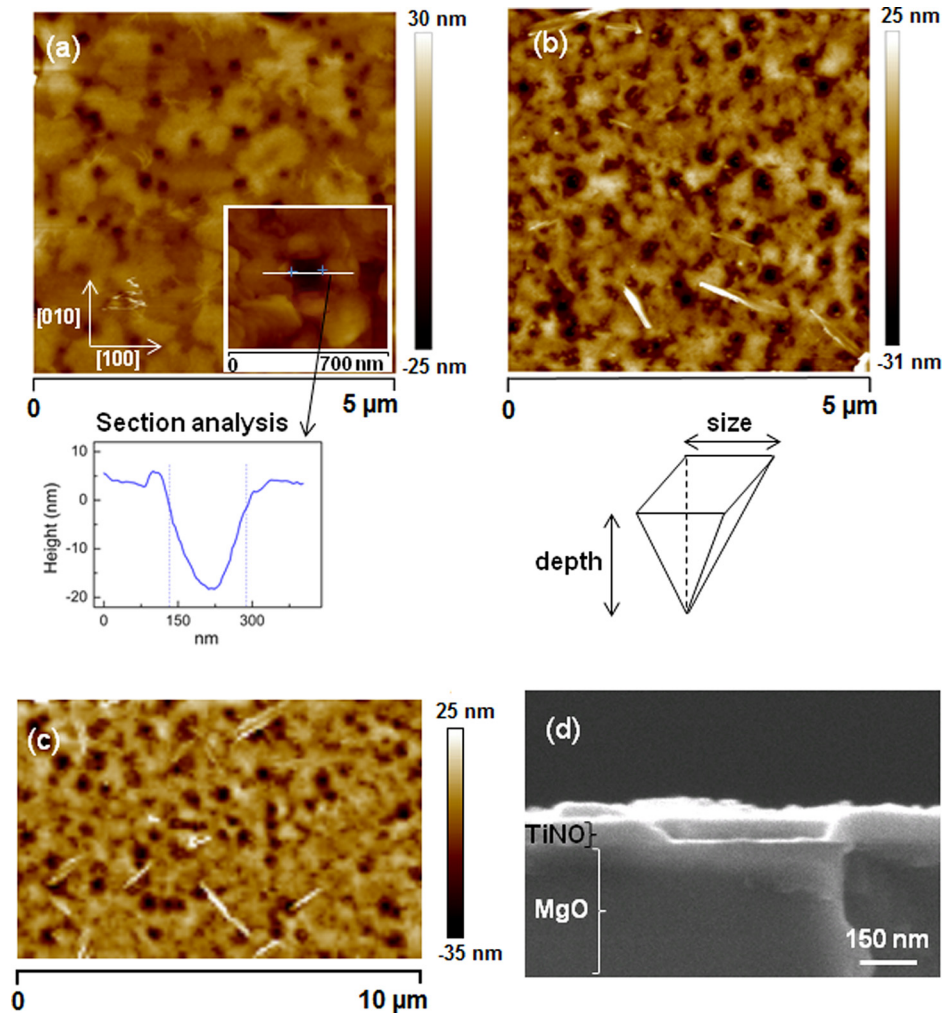


FIG. 2. (Color online) AFM images of TiNO after etching at (a) 8000 Pa for 1800 s (sample B), 10700 Pa for (b) 1800 s (sample C), and (c) 3600 s (sample D); (d) cross-sectional SEM image of TiNO after etching at 10700 Pa for 9000 s (sample E). The etch size and etch depth are defined in the drawing of the pyramid.

average etch size and etch depth increase from 141 nm and  $\sim 15$  nm to 175 nm and 20 nm, respectively, when pressure increases from 8000 Pa to 10700 Pa for the same etching time of 1800 s. For longer treatment (at 10700 Pa), the average etch size increases to 342 nm (3600 s) and 861 nm (9000 s), while the average etch depth increases to 34 nm (3600 s) and 76 nm (9000 s). The results reveal very low lateral and vertical etch rates of about  $78\text{--}95 \times 10^{-3}$  nm/s and  $8\text{--}9 \times 10^{-3}$  nm/s, respectively. Moreover, the lateral etch rate is much higher than the vertical etch rate ( $\sim 10$  times), indicating the preference for lateral etching of hydrogen plasma. Mandelson<sup>25</sup> has shown that in NaCl crystal, if the strained region around a dislocation is etched away or disappears, the etch pit is not etched further in depth but is enlarged laterally. Therefore, the anisotropic etching can be expected in TiNO as shown above. Cross-sectional SEM of sample E [Fig. 2(d)] shows the etch pit with a depth reaching the TiNO/MgO interface, implying that TiNO can be fully etched at 10700 Pa with etching time over 9000 s.

From the AFM images shown above, it is clear that TiNO films remain stable at hydrogen gas pressure under 5300 Pa, while etching occurs at pressure above 8000 Pa with the etch

rate increasing with pressure. It is also noticed that microwave plasma can produce a plasma density up to  $10^{12}$   $\text{cm}^{-3}$  much higher than that in RF plasma.<sup>24</sup> Hence, microwave plasma is more useful for the etch study because it may have faster etching rate under the etching condition as above. Moreover, TiNO is stable under pressure below 5300 Pa of microwave plasma, indicating that TiNO can survive in RF plasma which has been widely used in many industrial processing.

Exploration of the etch mechanism of TiNO film under hydrogen plasma may be helpful for understanding the effects of pressure and treatment time. The possible etch mechanism can be proposed based on thermodynamics, which allows us to define feasible chemical reactions which may occur in hydrogen plasma. As shown later in XPS data, as-grown TiNO films can be considered to consist of three components of titanium nitride, titanium oxynitride, and titanium dioxide. Moreover, hydrogen atoms and/or ions, generated by the dissociation of molecular hydrogen in plasma, are very powerful reductants that can reduce titanium oxide and nitride. Indeed, for example, at 1000 °C, the reduction of titanium oxide and nitride to the most common titanium hydride can be as the following:

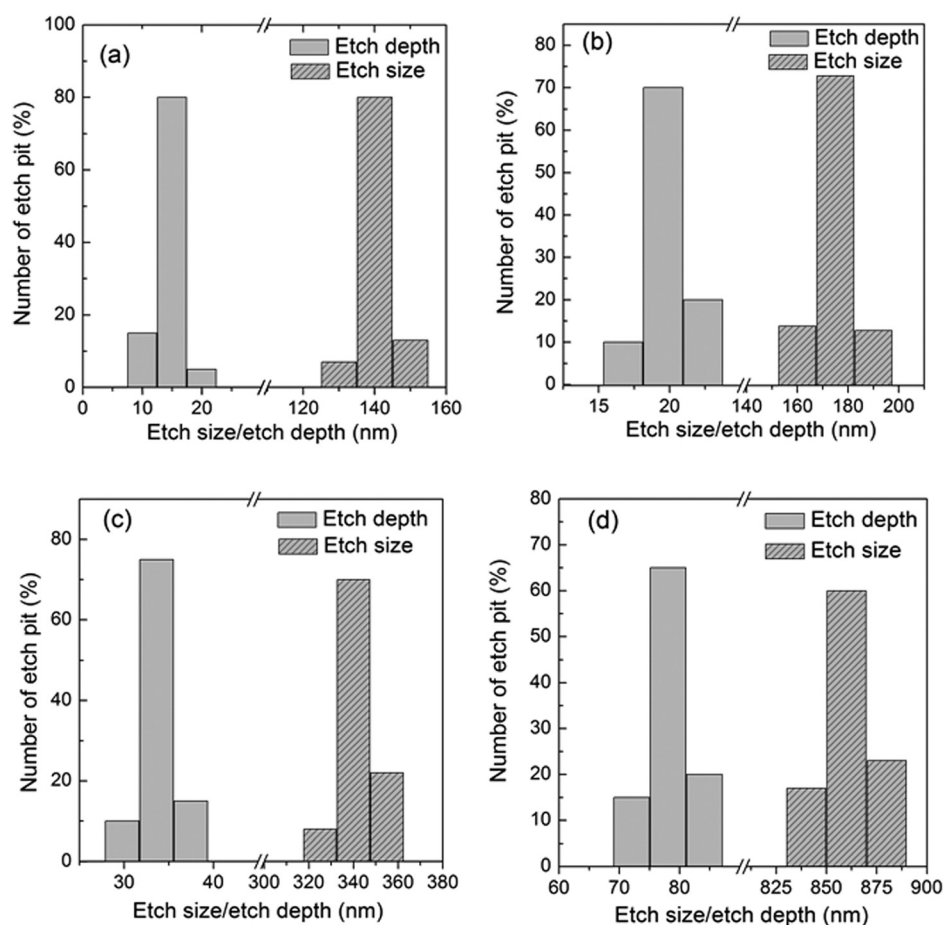
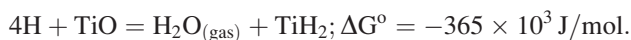
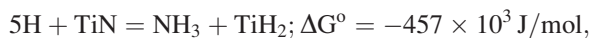
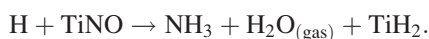


FIG. 3. Distribution of the etch size and etch depth after etching at (a) 8000 Pa for 1800 s, 10700 Pa for (b) 1800 s, (c) 3600 s, and (d) 9000 s.



All the reactions are thermodynamically favorable due to their negative Gibbs free energy  $\Delta G^\circ$  values.<sup>26</sup> Therefore, the reaction of TiNO in hydrogen plasma can be simply described as follows:



Titanium hydride ( $\text{TiH}_2$ ) has a relative low melting temperature of  $450^\circ\text{C}$ ; however, there is a lack of information on its vapor pressure. In general, a substance with low melting temperature has a high vapor pressure. Therefore,  $\text{TiH}_2$  could possess a high vapor pressure and it has a high tendency to desorb from the surface at substrate temperature as high as  $900\text{--}1100^\circ\text{C}$ . The stability and etching of TiNO can be now understood in terms of plasma density. Indeed, it is known that hydrogen plasma density increases with increasing pressure from 5300 to 10700 Pa.<sup>24</sup> Therefore, it may lead to the increase of ion and atomic hydrogen flux impinging on the TiNO surface as well as substrate temperature. As a consequence, the etching rate of TiNO can be enhanced by

increasing pressure. At hydrogen pressure of 5300 Pa, the etch rate could be so low that no etch pits are formed after 5400 s treatment time. When the pressure increased up to 8000 Pa, the etching rate was significantly enhanced, and the etch pits were then formed.

Again, it is noted that TiNO is almost intact under hydrogen plasma pressure below 5300 Pa. For a better understanding of stability of TiNO, chemical composition analyses for as-grown TiNO and sample A were performed by using XPS measurements. The XPS depth profiles in Fig. 4 reveal that the chemical composition of the TiNO film after plasma treatment at gas pressure of 5300 Pa remained unchanged with stoichiometry of  $\text{TiN}_{0.97}\text{O}_{0.23}$ . The oxygen in the as-grown film was not removed from the film by atomic hydrogen from plasma. The unchanged content of oxygen in sample A suggests that the properties of TiNO films are not affected by hydrogen plasma under pressure below 5300 Pa. High-resolution XPS spectra of Ti-2p and O-1s were examined to identify the chemical states of the as-grown TiNO and sample A (Fig. 5). As shown in Fig. 5(a), the Ti-2p spectrum of sample A reveals neither reduction of Ti to metallic state nor formation of  $\text{TiH}_2$  even at the surface region of TiNO film after hydrogen treatment. The Ti-2p peak can be deconvoluted into three components of titanium nitride (454.8 eV), titanium oxynitride ( $\sim 456.9$  eV), and titanium dioxide (458.5 eV).<sup>27</sup> After sputtering of the film surface for

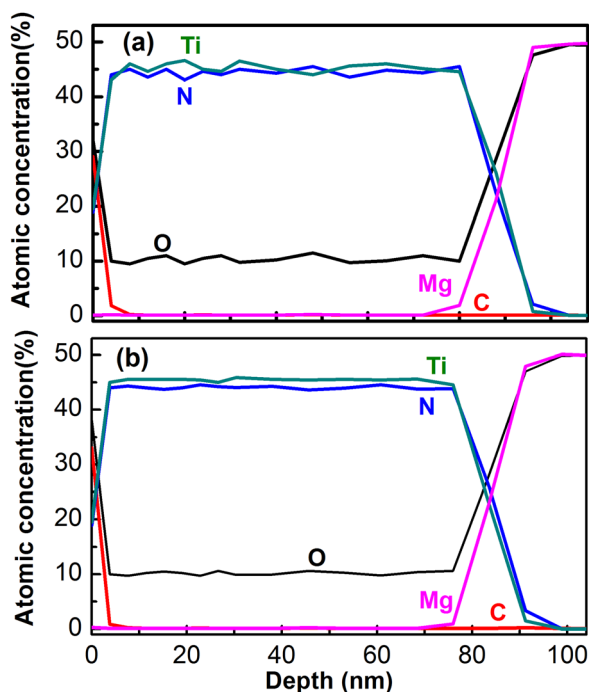


Fig. 4. (Color online) XPS depth profiles for (a) as-grown TiNO film and (b) sample A.

a few nanometers, the Ti-2p spectra of as-grown and treated TiNO films show exactly the same peak position and shape. The difference in the Ti-2p spectra between two samples is only found at the surface region, in which the as-grown film shows a much stronger TiO<sub>2</sub> signal compared with that of sample A. Therefore, the shift of Ti peak to higher oxidation state (TiO<sub>2</sub>) of the as-grown film surface is larger than that of the treated film. This implies that hydrogen plasma reduces the surface oxide in some extent. The decrease of TiO<sub>2</sub> signal at the surface region of the treated film may also suggest that hydrogen plasma treatment results in the surface passivation of TiNO that similar to the case of nitrogen/hydrogen plasma.<sup>18</sup> Figure 5(b) shows the corresponding O-1s spectra of as-grown and hydrogen plasma treated TiNO. In addition to titanium dioxide (530.5 eV) and titanium oxynitride (531.5 eV),<sup>27</sup> the surface region of the as-grown film also shows a component at 532.8 eV that can be assigned to the surface contamination (CO and C-OH) or Ti-OH groups.<sup>28,29</sup> After hydrogen plasma treatment at 5300 Pa, the surface of the treated film shows a strong and broaden peak at ~532.8 eV that can be explained by the enhancement of Ti-OH groups. The above XPS results provide strong evidence that TiNO is very chemically stable in hydrogen microwave plasma under pressure below 5300 Pa and atomic hydrogen from plasma affects mostly on the surface region of TiNO film.

The stability of TiNO was also investigated by using x-ray diffraction. As seen in Fig. 6, typical XRD patterns of as-grown TiNO and sample A show only (002) and (004) reflections of TiNO and MgO. No extra peaks such as Ti and TiH<sub>2</sub> are detected for treated TiNO films, indicating that TiNO remains stable under hydrogen plasma treatment for

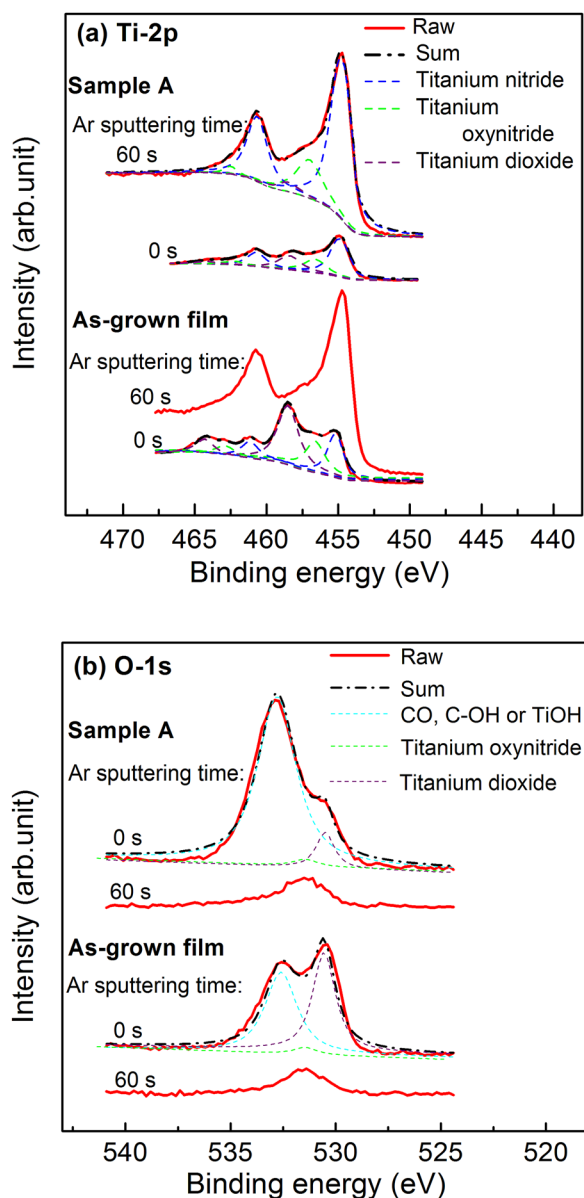


Fig. 5. (Color online) High-resolution XPS spectra for (a) Ti-2p and (b) O-1s as function of Ar sputtering time of as-grown TiNO and sample A. The spectra were deconvoluted into components using Voigt curve fitting.

5400 s at pressure of 5300 Pa consistent with the XPS result above. The inset of Fig. 6 also shows that the full width at half maximum of the rocking curve of (002) TiNO for sample A after hydrogen plasma treatment increased slightly from 230 arcsec to 280 arcsec. The d-spacing of (004) TiNO for the as-grown and treated TiNO films are determined as 0.10636 and 0.10639 nm, respectively. No apparent change in the d-spacing, together with the stability of chemical composition, indicates that the thermal effect of plasma treatment has not caused any noticeable change in the strain state of TiNO (-0.69%) in spite of the treatment at high-temperature. The x-ray reflectivity curves of as-grown sample and sample A (Fig. 7) show also no difference in the critical angle and distance between period of the interference fringes, indicating no change in the density and thickness of

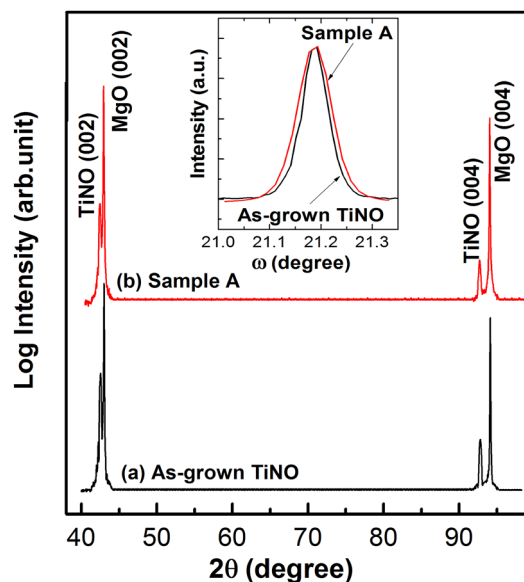


Fig. 6. (Color online) XRD  $2\theta$ - $\theta$  scans for (a) as-grown TiNO and (b) sample A. The corresponding XRD  $\omega$ -scan of (002) TiNO is displayed in the inset.

the TiNO films after treatment at hydrogen pressure below 5300 Pa, respectively. The decrease of the fringe intensity suggests that the TiNO surface is rougher after plasma treatment. However, the hydrogen plasma treatment had no effect on the TiNO/MgO interface because any increase in interface roughness will cause fringe amplitude to fall off more quickly with increasing scattering angle and may smear out the fringes. Analysis of interference fringes gives thickness and interface roughness of 76 and 0.2 nm for both samples; and surface roughness of as-grown and treated films can be determined as 0.3 and 0.4 nm in agreement with the AFM result. It has been shown that MgO is easily etched if the surface is in direct exposure to the plasma containing atomic hydrogen.<sup>30</sup> Therefore, the sharp interface still remained after plasma treatment implies that MgO can be protected by the TiNO in microwave hydrogen plasma under pressure

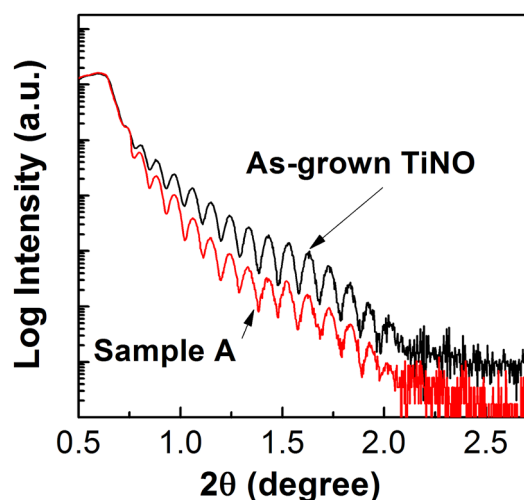


Fig. 7. (Color online) X-ray reflectivity curves for TiNO films before and after treatment at 5300 Pa for 5400 s.

below 5300 Pa. The XRD patterns for the etched samples B, C, D, and E also show (002) and (004) reflections of TiNO with almost unchanged d-spacing, implying that the non-etched region still remains to be TiNO.

#### IV. SUMMARY AND CONCLUSIONS

It has been demonstrated that titanium oxynitride is very chemically and thermally stable in microwave hydrogen plasma under pressure below 5300 Pa; XPS and XRD provide strong evidence that the chemistry and crystallinity of 76 nm thick TiNO films in plasma are almost intact. The etch pits with inverse pyramid shape are found to occur on (001)TiNO surface at pressure as high as 8000 Pa. AFM examinations reveal that the etch size and etch depth increase with increased etching time and pressure.

#### ACKNOWLEDGMENT

The work was supported by National Science Council, Taiwan, R.O.C. under Contract No. NSC 98-2221-E-009-042-MY3.

- <sup>1</sup>H. O. Pierson, *Handbook of Refractory Carbides and Nitrides: Properties, Characteristics, Processing and Applications* (Noyes Publication, Westwood, NJ, 1996).
- <sup>2</sup>W. D. Sproul and R. Rothstein, *Thin Solid Films* **126**, 257 (1985).
- <sup>3</sup>S. R. Min, H. N. Cho, Y. L. Li, S. K. Lim, S. P. Choi, and C. W. Chung, *J. Ind. Eng. Chem.* **14**, 297 (2008).
- <sup>4</sup>C. Ernsberger, J. Nickerson, A. E. Miller, and J. Moulder, *J. Vac. Sci. Technol. A* **3**, 2415 (1985).
- <sup>5</sup>F. Fracassi, R. D'Agostino, R. Lamendola, and I. Mangieri, *J. Vac. Sci. Technol. A* **13**, 335 (1995).
- <sup>6</sup>S. C. Abraham, C. T. Gabriel, and J. Zheng, *J. Vac. Sci. Technol. A* **15**, 702 (1997).
- <sup>7</sup>S. Benhenda, J. M. Guglielmacchi, M. Gillet, L. Hultman, and J.-E. Sundgren, *Appl. Surf. Sci.* **40**, 121 (1989).
- <sup>8</sup>S. P. Murarka and S. W. Hymes, *CRC Crit. Rev. Solid State Mater. Sci.* **20**, 87 (1995).
- <sup>9</sup>M. Rocke and M. Schneegans, *J. Vac. Sci. Technol. B* **6**, 1113 (1988).
- <sup>10</sup>V. D. Kulkarni and N. C. Sharma, *J. Electrochem. Soc.* **135**, 3094 (1988).
- <sup>11</sup>S. Miyaji, T. Kato, and T. Yamauchi, *J. Vac. Sci. Technol. A* **14**, 3082 (1996).
- <sup>12</sup>N. Biunno, J. Narayan, S. K. Hofmeister, A. R. Srivatsa, and R. K. Singh, *Appl. Phys. Lett.* **54**, 1519 (1989).
- <sup>13</sup>R. Chowdhury, R. D. Vispute, K. Jagannadham, and J. Narayan, *J. Mater. Res.* **11**, 1458 (1996).
- <sup>14</sup>M. Danek, M. Liao, J. Tseng, K. Littau, D. Saigal, H. Zhang, R. Moseley, and M. Eizenberg, *Appl. Phys. Lett.* **68**, 1015 (1996).
- <sup>15</sup>N. Kumar, J. T. McGinn, K. Pourrezaei, B. Lee, and E. C. Douglas, *J. Vac. Sci. Technol. A* **6**, 1602 (1988).
- <sup>16</sup>P. Jin and S. Maruno, *Jpn. J. Appl. Phys.* **30**, 2058 (1991).
- <sup>17</sup>R. Kröger, M. Eizenberg, C. Marcadal, and L. Chen, *J. Appl. Phys.* **91**, 5149 (2002).
- <sup>18</sup>J. K. Huang, C. L. Huang, S. C. Chang, Y. L. Cheng, and Y. L. Wang, *Thin Solid Films* **519**, 4948 (2011).
- <sup>19</sup>H. Kawamoto, H. Sakaue, S. Takehiro, and Y. Horiike, *Jpn. J. Appl. Phys.* **29**, 2657 (1990).
- <sup>20</sup>J. Tonotani, T. Iwamoto, F. Sato, K. Hattori, S. Ohmi, and H. Iwai, *J. Vac. Sci. Technol. B* **21**, 2163 (2003).
- <sup>21</sup>R. N. Tiwari and L. Chang, *Semicond. Sci. Technol.* **25**, 035010 (2010).
- <sup>22</sup>H. Do, Y.-H. Wu, V.-T. Dai, C.-Y. Peng, T.-C. Yen, and L. Chang, *Surf. Coat. Technol.* **214**, 91 (2013).
- <sup>23</sup>V. G. Ralchenko, A. A. Smolin, V. I. Konov, K. F. Sergeichev, I. A. Sychov, I. I. Vlasov, V. V. Migulin, S. V. Voronina, and A. V. Khomich, *Diamond Relat. Mater.* **6**, 417 (1997).

<sup>24</sup>Oleg A. Popov, *High Density Plasma Sources: Design, Physics and Performance* (Noyes Publications, NJ, 1995).

<sup>25</sup>S. Mendelson, *J. Appl. Phys.* **32**, 1579 (1961).

<sup>26</sup>M. W. Chase, Jr., *NIST-JANAF Thermochemical Tables* (American Institute of Physics, New York, 1998).

<sup>27</sup>M. H. Chan and F. H. Lu, *Surf. Coat. Technol.* **203**, 614 (2008).

<sup>28</sup>T. K. Sham and M. S. Lazarus, *Chem. Phys. Lett.* **68**, 426 (1979).

<sup>29</sup>T. Kasuga, H. Kondo, and M. Nogami, *J. Cryst. Growth* **235**, 235 (2002).

<sup>30</sup>K. H. Baik, P. Y. Park, B. P. Gila, J. H. Shin, C. R. Abernathy, S. Norasethekul, and S. J. Pearton, *Appl. Surf. Sci.* **183**, 26 (2001).